Comparison of DC-Link Voltage Control Architectures on Grid-Side and Machine-Side for Permanent Magnet Synchronous Generator Connected to the Grid

Molina Gordillo, Steven Xavier y Santo Chiluisa, Marco Antonio

Departamento de Eléctrica y Electrónica

Carrera de Ingeniería Electrónica e Instrumentación

Artículo académico, previo a la obtención del título de Ingeniera en Electrónica e Instrumentación

Ing. Llanos Proaño, Jacqueline del Rosario MSc. PhD

15 de agosto del 2022

Latacunga

Comparison of DC-Link Voltage Control Architectures on Grid-Side and Machine-Side for Permanent Magnet Synchronous Generator Connected to the Grid

Steven Molina
Eléctrica y Electrónica
Universidad de las Fuerzas Armadas
ESPE
Sangolquí-Ecuador
sxmolina@espe.edu.ec

Marco Santo
Eléctrica y Electrónica
Universidad de las Fuerzas Armadas
ESPE
Sangolquí-Ecuador
masanto1@espe.edu.ec

Jacqueline Llanos
Eléctrica y Electrónica
Universidad de las Fuerzas Armadas
ESPE
Sangolquí-Ecuador
jdllanos1@espe.edu.ec

Jorge Vega
Eléctrica
Universidad de Antofagasta
Antofagasta-Chile
jorge.vega@uantof.cl

Franklin Silva
Eléctrica y Electrónica
Universidad de las Fuerzas Armadas
ESPE
Sangolquí-Ecuador
fmsilva@espe.edu.ec

***Abstract*—Energy production through wind power generation systems presents instability mainly due to wind variability the dynamic performance of the DC-Link is necessary for the proper operation of wind power plants using PMSG-based technologies, therefore, it is necessary to guarantee the efficient voltage control in the DC-Link in a back to back topology of the converters used for the energy conversion. This research compares the effect of implementing DC-Link voltage control on the Grid Side Converter versus DC-Link voltage control on the Machine Side Converter. The simulated system consists of a wind turbine coupled to the Permanent Magnet Synchronous Generator, Power Electronic Converters and the grid. Internal current controllers and external DC-link voltage control are designed for each case. The performance of the system against wind speed changes and voltage faults in the grid is evaluated and compared.**

Keywords—DC-link, Grid Side Converter, Machine Side Converter, wind system, wind turbines.

I. INTRODUCTION

Electric energy is necessary for world progress, since it allows the social and economic development of the population [1]. The electricity demand has been increasing until it has become a problema. This is because energy sources from non-renewable resources have been used, generating short- and long-term environmental issues to supply the electricity demand [2]. Wind energy is considered a renewable resource that helps to mitigate these issues.

Global wind power generation in 2021 was 1814 TWh, representing 6.6% of the world's electrical energy, with China being the leader in wind energy generation with 148 TWh [3]. In Latin America, there has also been a constant increase in wind energy installed capacity. For example, the installed wind power capacity of Brazil in 2021 was 21161 MW [4], 3137 MW in Chile [4][5], and 3292 MW in Argentina [4][6]. Furthermore, [4][7] establish that 81.02% of the total energy production in Ecuador is renewable energy, where 0.24% is produced by wind farms with an installed wind capacity of 21.15 MW in 2021.

Wind systems have had significant developments with the use of high-power wind turbines and flexible structures. However, the main problem of this type of system is presented when trying to obtain energy in wind turbines as they maintain a cubic relationship with the wind speed, where the variation in speed produces energy fluctuations and make it difficult to operate the system [8][9], therefore, it is necessary to use power converters and controllers design in order to adapt the signal delivered by the wind turbine, and provide a constant signal in both amplitude and frequency for injection into the power grid [10][11].

Different solutions have been proposed from the point of view of power electronics and process control. In [12], power converter topologies are proposed to provide high reliability, redundancy, and better power quality. Back-to-back converters are the most used among the topologies studied due to their interconnection of the electric power grid with different machines or electric loads [13][14]. In [15] presents the power regulation produced by a wind turbine rotation speed control and conventional control schemes of a three-phase wind generation system connected to the electric power grid. In [16], wind farm stability problems are examined by analytical models in which active power control and DC-link voltage control are assumed to demonstrate the most efficient approach. In [17], a dc bus voltage control for a large-scale wind turbine connected to a dc grid is developed.

In [18], a non-linear disturbance observer (NDO) is proposed to improve the dynamic performance of the voltage source converter (VSC). A feedforward with a voltage control loop is considered, which suppresses the transient variations of the DC-link voltage, improving the VSC dynamics and the power quality of the system.

There are different technologies associated with wind energy production in order to transform mechanical energy into electrical energy such as: fixed speed induction generator[19], permanent magnet synchronous generator (PMSG) [20], doubly fed induction generator (DFIG) [21], and variable speed synchronous generator [22]. In this research, the PMSG is selected because when generating

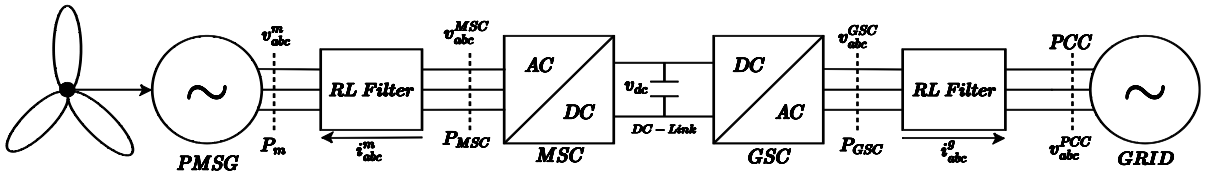

Fig. 1. Diagram of a WECS based on PMSG

voltages at low wind speeds, it is unnecessary to use a gearbox, requires less maintenance, provides greater reliability, and has improved overall performance [23] [24].

This research models a wind turbine coupled to a PMSG without a multiplier box connected to the grid with a 2-Level converter in a back-to-back configuration. In addition, a PLL based on a synchronous reference frame, current controllers for the grid side converter (GSC), and the machine side converter (MSC) are designed, all based on the d-q reference frame. Two control architectures are applied to this system. In the first case, voltage regulation on the DC-link controlled is implemented from GSC, and in the second case, voltage control on the DC-link is implemented on the MSC. For this purpose , dynamic simulations, parameter selection , and analytical models of grid interconnection are used. After analyzing and comparing the performance of the controllers in the two cases, the best of them will be selected,. The selection considers dynamic performance indexes such as the settling time, overshoot, and steady-state error in the voltage control variable in the DC-link, also the power delivered to the grid at the point of common coupling (PCC) is validated for the two implemented cases. Finally, tests will be performed simulating voltage failures in the power grid to verify the correct operation of the controllers against these disturbances.

The main contribution of this research work is to compare and identify the most efficient control architecture for the dynamic performance of the wind generation unit, in order to guarantee a constant voltage in the DC-link in the face of wind speed changes and possible overvoltages or voltage drops, taking advantage of the wind resource that is reflected in the amount of power delivered to the grid.

II. Wind Turbine Model

The Wind Energy Conversion System (WECS) shown in Fig. 1, is composed of a PMSG generator, voltage source converter (VSC) in back-to-back configuration (MSC and GSC), filters of L type, and a DC-link capacitor. The wind system is connected to the grid through the Point of Common Coupling (PCC). Each part of the model is described below.

A. PMSG Model

The Park model is a common model of PMSG generator in the d-q reference frame [25], the stator voltage in d-q references frame (v_d^m and v_q^m) are defined by (1) and (2), respectively. Where i_{sd} is the stator current. ψ_{sd} and ψ_{sq}, are the stator fluxes in d-q references frame generated by the machine due to its magnets, defined by (3) and (4). R_S is the stator winding resistance, ω_e represents the angular frequency of the rotating shaft associated with the d-q axes. L_S is the leakage inductance of the PMSG.

$$v_d^m = -R_s i_{sd} - \frac{d\psi_{sd}}{dt} - \omega_e \psi_{sq} \quad (1)$$

$$v_q^m = -R_s i_{sd} - \frac{d\psi_{sq}}{dt} + \omega_e \psi_{sd} \quad (2)$$

$$\psi_{sd} = L_s i_{sd} + \psi_{fd} \quad (3)$$

$$\psi_{sq} = L_s i_{sq} + \psi_{fq} \quad (4)$$

Replacing (3) and (4) in (2) and (1) respectively, the following equations are obtained:

$$v_d^m = -R_s i_{sd} - \frac{d\psi_{sd}}{dt} - \omega_e L_s i_{sq} - \omega_e \psi_{fq} \quad (5)$$

$$v_q^m = -R_s i_{sd} - \frac{d\psi_{sq}}{dt} + \omega_e L_s i_{sd} - \omega_e \psi_{fd} \quad (6)$$

In [26] it is mentioned that, superficial magnet PMSG generators possess uniform air gap, thus, the inductances in d-q are identical. If steady state analysis is performed, then $\frac{d\psi_{sd}}{dt} = 0$, and $\frac{d\psi_{sq}}{dt} = 0$. $R_S \approx 0\,\Omega$ and $L_S \approx 0\,H$, are considered due to the PMSG is modeled as rotational velocity dependent sources, equations (7) and (8) are obtained:

$$v_d^m = -\omega_e \psi_{fq} \quad (7)$$

$$v_q^m = \omega_e \psi_{fd} \quad (8)$$

III. DC-link voltage controller design applied to Grid Side Converter

Cascade control is performed for both GSC and MSC. It comprises inner current control loops and outer voltage control loops in the DC-link. Additionally, a PLL is used for the synchronization method. The inner control loops are faster than the outer control loop, which means that they operate at different bandwidths [27]. Consequently, the design of the controller can be done separately.

A. Design of Current Controllers

Fig 2 shows the implemented controllers on the GSC. On the right side, the implementation of the voltage control in the DC-link can be observed. The design of current controllers is described in detail below.

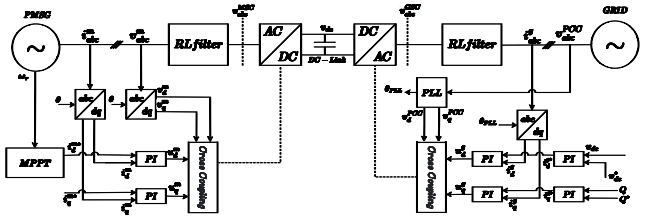

Fig. 2. General diagram for DC-link voltage control on GSC

Vector control is used and implemented in d-q reference frame. The control is oriented to the voltage at PCC $\left(v_d^{PCC}, v_q^{PCC}\right)$ [27].

The circuit shown in Fig. 3 represents the GSC, it is used to determine the model and obtain the gains of the Proportional Integral (PI) current controllers. In Fig. 3 the GSC voltage and the current flowing from the GSC node to the PCC are denoted as v_{abc}^{GSC} and i_{abc}^{g}, respectively. The voltage at the coupling point is denoted as v_{abc}^{PCC}. An RL circuit between the converter and the grid is considered. Applying Kirchhoff Voltage Law (KVL), equation (9) is obtained.

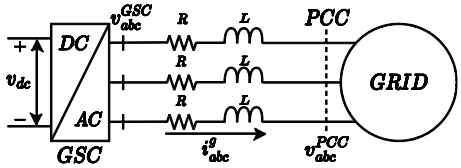

Fig. 3. Circuit diagram of the converter connected to the grid.

$$v_{abc}^{GSC} - v_{abc}^{PCC} = L\frac{di_{abc}^{g}}{dt} + Ri_{abc}^{g} \tag{9}$$

Equation (10) shows the representation in d-q references frame:

$$\begin{aligned}&(v_d^{GSC} + jv_q^{GSC}) - (v_d^{PCC} + jv_q^{PCC}) = \\ &L\frac{d(i_d^g + ji_d^g)}{dt} + j\omega_0 L(i_d^g + ji_d^g) + R(i_d^g + ji_d^g)\end{aligned} \tag{10}$$

Where $v_q^{GSC} = 0$ because the PCC voltage is oriented towards the d-axis and ω_0 is the grid angular frequency.

By separating equation (10) into d-q axes, the model for the controller design is obtained for (11) and (12).

$$L\frac{di_d^g}{dt} + Ri_d^g = \underbrace{v_d^{GSC} - v_d^{PCC} + \omega_0 Li_q^g}_{u_d} \tag{11}$$

$$L\frac{di_q^g}{dt} + Ri_q^g = \underbrace{v_q^{GSC} - v_q^{PCC} + \omega_0 Li_d^g}_{u_q} \tag{12}$$

Fig 4 shows shows the closed-loop control system for current control. The PI controller gives the plant model for d-q references frame includes the tuning gains K_p and K_i.

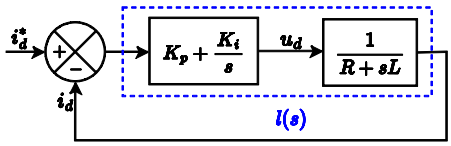

Fig. 4. Block diagram of current inner loop control.

The input signals to the plant are u_d and u_q, which represent the control actions, and the outputs i_d^g and i_q^g are the variables to be controlled. In addition, the cross-coupled components and direct supply voltage are integrated into the controller output in order to generate the d-q voltage components of the converter [27] as shown in Fig. 6. From Fig. 4, the direct gain of the system $l(s)$ is given by (13).

$$l(s) = \frac{K_p}{sL}\left(\frac{s + K_i/K_p}{s + R/L}\right) \tag{13}$$

The plant pole is very close to the origin, so it is canceled by the zero, $\left(\frac{K_i}{K_p} = \frac{R}{L}\right)$, therefore, $l(s)$ is represented by (14) [27].

$$l(s) = \frac{K_p}{sL} \tag{14}$$

Then, the transfer function of the closed-loop system is denoted by (15). Where: $\tau = \frac{L}{K_p}$ and $K_i = \frac{R}{\tau}$.

$$G(s) = \frac{l(s)}{1 + l(s)} = \frac{1}{\tau s + 1} \tag{15}$$

B. *Phase-Locked Loop (PLL) Design*

A second-order PLL is designed as shown in Fig. 5. The inputs are three-phase voltages, which are transformed into their d-q references frame as a function of the angle θ_{PLL}. A PI controller is provided to ensure that the voltage on the q-axis is zero [28].

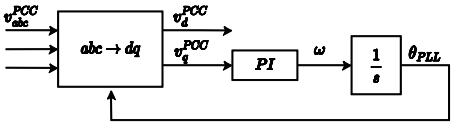

Fig. 5. PLL Block Diagram

C. *Maximum Power Point Tracking (MPPT)*

In this research, the external loop is not considered to control the power, but the relationship between the machine's rotational speed and the active power, defined by (16), is considered. Where, P_m is the active power generated (Fig. 1), ω_r is the rotational mechanical speed of the generator, which is measured in rpm and K_{opt} is a constant that depends on the sweep profile of the blades, wind density and others.

$$P_m = K_{opt}\omega_r^3 \tag{16}$$

D. *DC-link voltage controller Design*

A first-order model describes the dynamics associated with the DC-link's capacitor [29]. It should be considered that DC-link voltage equation (v_{dc}) showed in [29] is expressed in per unit (pu). For this research real values are used. Where, (17) represents the dynamics of the DC-Link, P_{MSC} and P_{GSC} are the active power in MSC (18) and GSC (19) respectively.

$$Cv_{dc}\frac{dv_{dc}}{dt} = P_{MSC} - P_{GSC} \tag{17}$$

$$P_{MSC} = \frac{3}{2}\left(v_d^{MSC}i_d^g + v_q^{MSC}i_q^g\right) \tag{18}$$

$$P_{GSC} = \frac{3}{2}\left(v_d^{GSC}i_q^g - v_q^{GSC}i_d^g\right) \tag{19}$$

Fig. 6a shows the control scheme for the voltage on the DC-link when it is implemented in the GSC. The objective control is to maintain the measured DC-link voltage (v_{dc}) at the desired value v_{dc}^*. The voltage controller in the DC-link is defined by $Kp_{DC} + \frac{Ki_{DC}}{s}$, the output i_d^{g*} is the reference current

for current control. Fig. 6b shows the implemented controllers for the MSC, where the MPPT output i_d^{m*} is the reference current for the current controller and ω_e is the machine frequency angular.

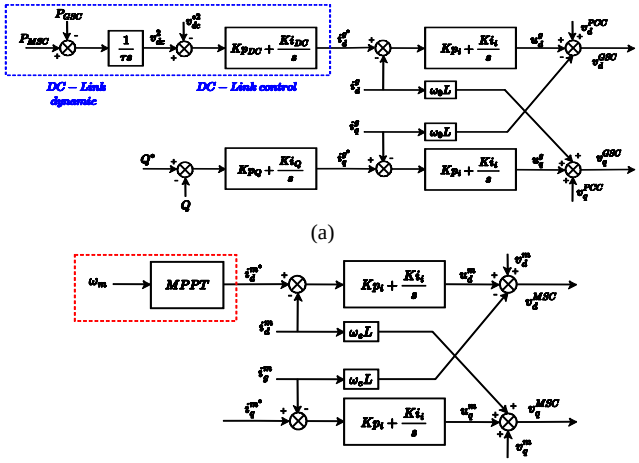

(a)

(b)

Fig. 6. DC-link voltage control scheme on GSC (a) GSC (b) MSC.

IV. DC-LINK VOLTAGE CONTROLLER DESIGN APPLIED TO MACHINE SIDE CONVERTER

The same PI controllers obtained in Section III are considered for the DC-link control scheme on the machine side, the PI controllers of the DC-link voltage in MSC are added. As shown in Fig. 7, the set points of the current controllers i_d^{m*} and i_d^{g*} are modified, where i_d^{m*} is defined by the voltage DC-link control. At the same time, i_d^{g*} is set by the MPPT. In contrast to the control architecture in Fig 6, the DC-link voltage control is implemented in MSC, as shown in Fig. 8.

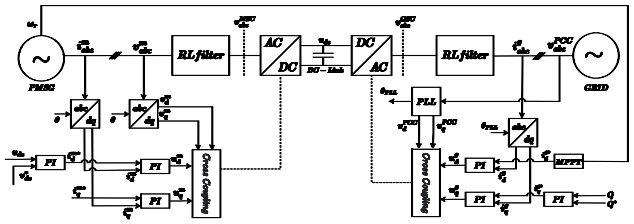

Fig. 7. General diagram for DC-link voltage control on MSC.

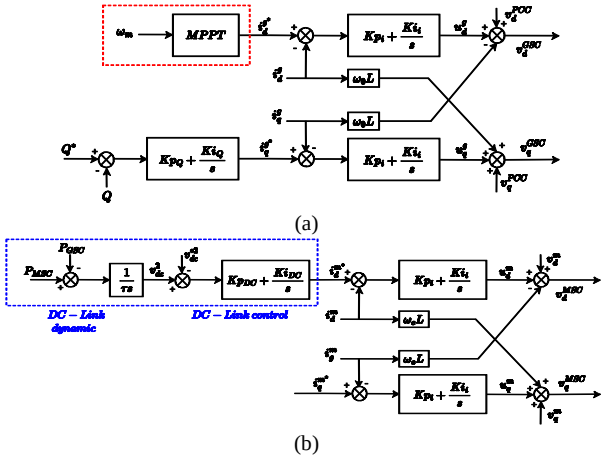

(a)

(b)

Fig. 8. DC-link voltage control scheme on MSC (a) GSC (b) MSC

V. RESULTS

The model for a PMSG with its control systems presented in previous sections are implemented in MATLAB/Simulink to perform time domain simulations. The bandwidths for current and DC voltage control are 628.32 rad/s and 10 rad/s respectively. The system parameters and control gains are shown in Table I.

TABLE I. SYSTEM PARAMETERS AND CONTROLLER GAINS

Description	Parameters	Values
Grid phase voltage (peak value)	v_{abc}^{g}	$400v$
Grid frequency	f_g	$60\,Hz$
Resistor (Filter)	R	0.25Ω
Inductante (Filter)	L	$0.007\,H$
DC-link voltage	V_{dc}	$1200v$
Machine Constant	K_{opt}	0,0001778
DC-link capacitor	C	$0.001\,F$
Current control	(Kp_i, Ki_i)	(4.398,157.079)
PLL control	(Kp_{PLL}, Ki_{PLL})	(125.66, 394784.176)
DC-link control	(Kp_{DC}, Ki_{DC})	(3.22,126.4)

This section evaluates the performance of the two DC-link voltage control architectures. In the first architecture the control is performed in the GSC (see Fig. 2) and the second one is when the control is implemented in the MSC (See Figure 7).

Two changes in angular velocity are applied ($\omega_r = 400\,rpm$ and $\omega_r = 500\,rpm$) to the two architectures, representing changes in wind speed. Fig. 9 and Fig. 10, shows the performance of the machine side and grid side currents when DC-link voltage control on GSC and on MSC, respectively.

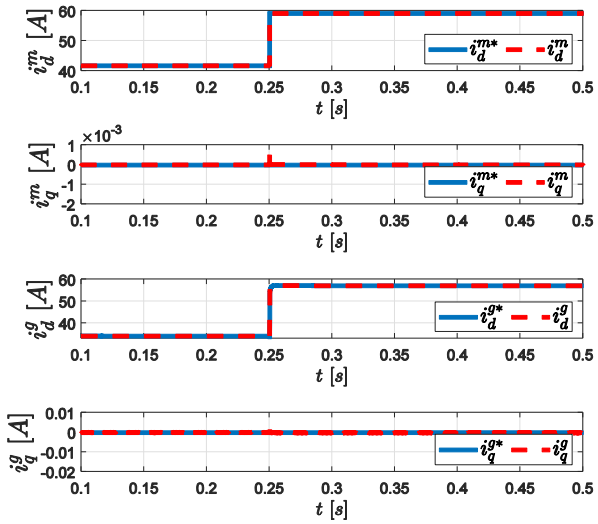

Fig. 9. Machine and generator current when DC-link voltage control on GSC.

The grid side d-q references frame currents $\left(i_d^g, i_q^g\right)$ have similar performance in both cases, they do not present overshoot. On the other hand, the machine-side d-q currents $\left(i_d^m, i_q^m\right)$ are adequately controlled. However, the i_d^m current presents an overshoot of 4.97% (see Fig. 10).

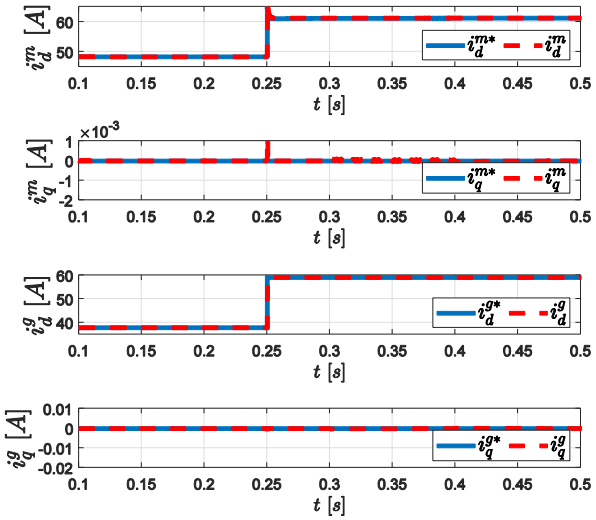

Fig. 10. Machine and generator current when DC-link voltage control on MSC.

Thus, the machine-side current control in d- reference frame shows better performance when the DC-link voltage is implemented in GSC.

Fig. 11 shows the performance of the DC-link voltage controllers, and it can be observed that when the wind change occurs in both architecture the voltage stabilizes at the Set Point (SP) of 1200V. The DC-link voltage when the control is on GSC has a 0.000225% of overshoot and 0.000225% of overshoot when the control is on MSC. These values are very small.

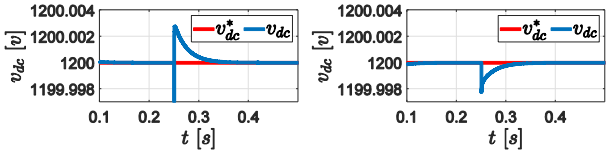

(a) (b)

Fig. 11. DC-link voltage control. (a) DC-link voltage control on GSC (b) DC-link voltage control on MSC.

Fig. 12, shows the power supplied to the grid at the PCC for the two architectures. It can be seen that when the voltage of DC-link is controlled in MSC, the active power is greater than that obtained from the DC-link voltage control architecture in GSC, because the MPPT extracts all the power from the generator and defines the current set point ($i_d^{g^*}$) of the GSC. Less active power is available when the voltage of DC-link control is in GSC since because the DC-link control gives the current, it is important to consider that the DC-link dynamic is directly related to the power in MSC as shown in (18).

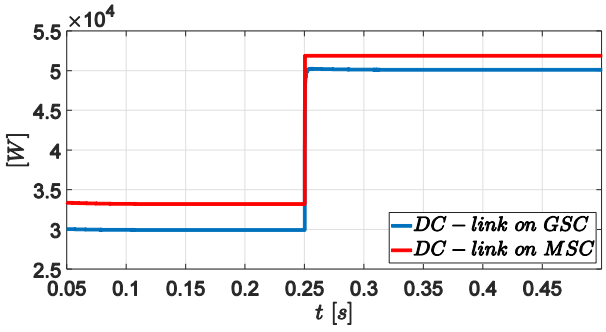

Fig. 12. Active Power on PCC

In addition, a grid failure (50% reduction of v_{abc}^g) was simulated for a time t=0.1 s in order to test the robustness of the controllers. The voltage at v_{abc}^g is shown in Fig. 13.

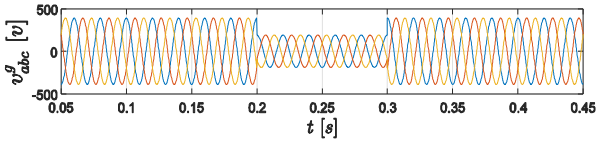

Fig. 13. 50% reduction in grid voltage (v_{abc}^g).

Fig. 14 and Fig. 15, shows the performance of the controllers against a voltage drop in the grid. When the DC-link voltage control is in GSC (Fig. 14), it can be observed that the current i_d^g increases its value during the voltage drop to compensate for the power loss in the PCC, the other currents (i_q^g, i_d^m, i_d^m) are maintained at their set point value. On the other hand, when the DC-link voltage control is in MSC (Fig. 15), it is observed that the current i_d^m reduces its value, this is because at the moment the fault occurs, the power in PCC reduces its value, therefore, the control objective of MSC is only to supply the necessary power to the grid, the other currents (i_d^g, i_q^g, i_q^m) maintain their set point value at the moment the fault occurs.

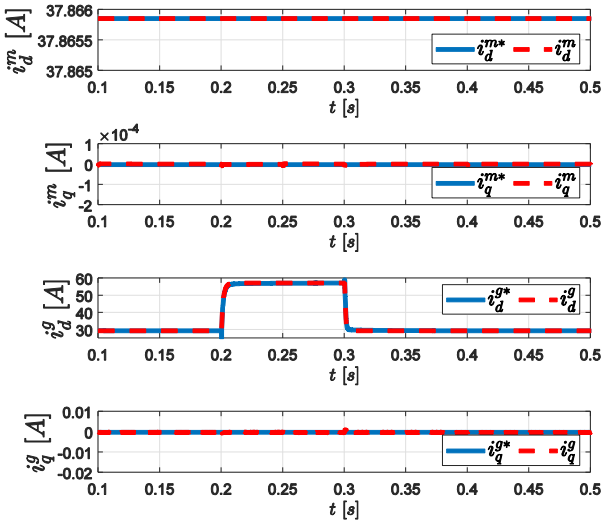

Fig. 14. d-q current control when a voltage drop occurs in the grid (DC-link voltage control on GSC).

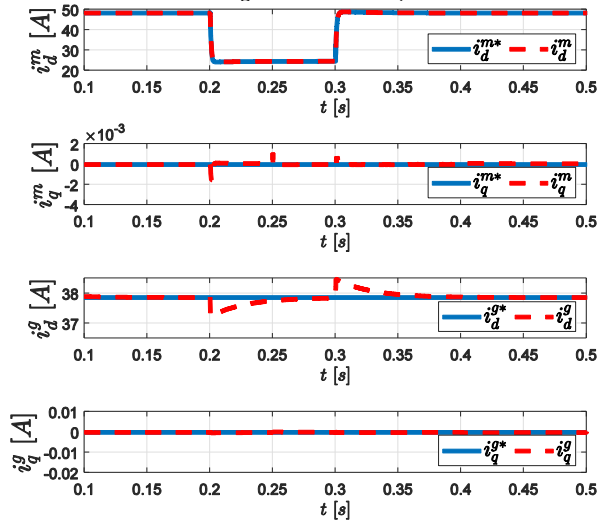

Fig. 15. d-q current control when a voltage drop occurs in the grid (DC-link voltage control on MSC).

Fig. 16 shows the performance of the DC-link voltage controllers, and it can be observed that when the disturbance in the grid occurs in both architecture the voltage stabilizes at the Set Point (SP) of 1200V. The DC-link voltage when the control is on GSC has a 0.000242% of overshoot and 0.000225%. of overshoot when the control is on MSC (Fig. 16b). These values are very small.

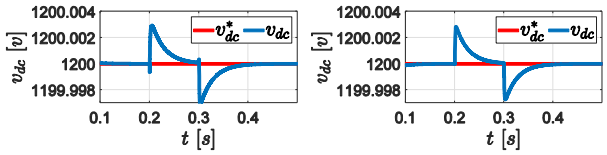

Fig. 16. DC-link voltage control when a voltage drop occurs in the grid. (a) DC-link voltage control on GSC (b) DC-link voltage control on MSC.

Fig. 17 shows the power at PCC, where it can be seen that the generator recovers after eliminating the voltage drop Global Electricity Review 2022 in the grid. The active power is still higher when the DC-link voltage is controlled at MSC, but at the fault instant it tends to be lower because the current $i_d^{g^*}$ is maintained at a set point given by the MPPT (Fig. 15), then the power at PCC depends directly on v_d^{PCC}. On the other hand, when the DC-link voltage is controlled at GSC, at the fault instant there is less power loss at PCC, since the current $i_d^{g^*}$ is given by the DC-link voltage control, which controls immediately (Fig. 16 a) and does not allow considerable losses in the current i_d^g.

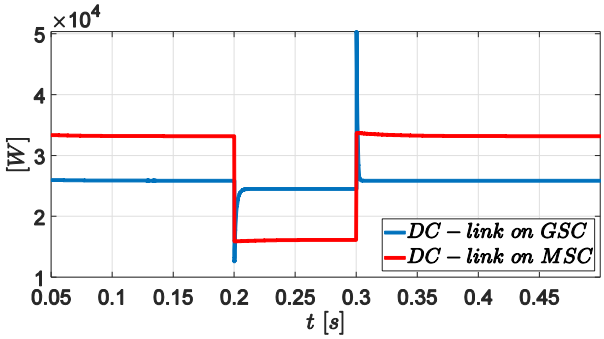

Fig. 17. Active power on PCC applying a disturbance in the grid.

VI. Conclusions

In this research, two DC-link voltage control architectures are implemented and compared by time domain simulations. The first was designed in GSC, and the second was designed in MSC. The comparison between the two architectures shows that when the DC-link voltage is controlled in MSC, more power is obtained in PCC than when it is controlled in GSC. This is because the MPPT sends the reference current directly to the GSC, so power losses that exist in MSC are not considered. Less power is obtained when the DC-link voltage is controlled at GSC because power losses at MSC and GSC are considered. Therefore, it is proposed to control the voltage DC-link from MSC to use wind energy better.

The voltage in the DC-link is maintained at the setpoint in both architectures when there are wind variations. The DC-link voltage shows a negligible overshoot when the control is implemented in GSC, likewise, when the control is implemented in MSC the DC-link voltage shows an undershoot. On the other hand, when there are faults in the grid, the control architectures manage to control themselves against this problem, presenting an overshoot of 0.000225% and 0.000166% when the DC-link voltage is controlled from the GSC and MSC, respectively.

Finally, it is verified that the two control architectures are stable since the current and voltage controllers respond correctly when wind variations occur at the input and grid faults occur. In the two architectures, good performance of the DC-link voltage is shown.

In future work, it is proposed to model the grid in more detail and design robust controls against weak bars (impedance in the grid). In addition, the wind turbine will design and implement pitch angle control.

References

[1] Organización de las Naciones Unidas, “Energía - Desarrollo Sostenible.” https://www.un.org/sustainabledevelopment/es/energy/ (accessed May 30, 2022).

[2] M. Armijos-Yambay, S. Camino-Mogro, P. Avilés-Terán, K. Parrales-Guerrero, and L. Herrera-Paltán, “Estudios Sectoriales: La Inversión Extranjera Directa y la Rentabilidad de las Compañias en el Ecuador 2013-2018,” *Dir. Nac. Investig. y Estud. la Supt. Compañias, valores y seguros del Ecuador*, pp. 1–30, 2020, [Online]. Available: https://investigacionyestudios.supercias.gob.ec/wp-content/uploads/2020/01/IED_rentabilidad_FINAL.pdf.

[3] D. Jones, E. Graham, P. Tunbridge, and A. Ilas, “Global Electricity Review 2022,” no. March, p. 75, 2022.

[4] IRENA, *Renewable Capacity Statistiques De Capacité Estadísticas De Capacidad*, 2021st ed. Masdar: United Arab Emirates, 2021.

[5] R. D. E. SPEC *et al.*, “Análisis y Propuesta de una Ruta de Referencia para alcanzar cero emisiones en el sector de generación de Energía Eléctrica en Chile,” Chile, 2021.

[6] G. Escala and J. A. Septiembre, “Energías Renovables,” Argentina, 2022.

[7] N. Renovables, “Edición 10 mayo 2022,” 2022.

[8] M. G. Molina, P. E. Mercado, and S. Juan, “Estrategia de control para maximizar la potencia extraída de aerogeneradores de velocidad variable conectados a la red eléctrica,” *Av. en energía Renov. y medio Ambient.*, vol. 12, pp. 65–72, 2008.

[9] S. Karyś and P. Stawczyk, “Cost-effective power converters for small wind turbines,” *Energies*, vol. 14, no. 18, 2021, doi: 10.3390/en14185906.

[10] M. B. Anwar, M. S. El Moursi, and W. Xiao, “Novel Power Smoothing and Generation Scheduling Strategies for a Hybrid Wind and Marine Current Turbine System,” *IEEE Trans. Power Syst.*, vol. 32, no. 2, pp. 1315–1326, 2017, doi: 10.1109/TPWRS.2016.2591723.

[11] T. Ackerman, Wind Power in Power Systems, 1st, ed. Stockholm, Sweden. 2005.

[12] S. Gautam, A. K. Yadav, and R. Gupta, “AC/DC/AC converter based on parallel AC/DC and cascaded multilevel DC/AC converter,” *2012 Students Conf. Eng. Syst. SCES 2012*, 2012, doi: 10.1109/SCES.2012.6199078.

[13] C. Nieves, F. Quizhpi, “Análisis De Rendimiento Del Conversor Back To Back para Generador Eólico Implementado En Los Laboratorios De Energía De La Universidad Politécnica Salesiana”, Eléctrica, UPS, Cuenca, 2022.

[14] H. T. Ma, P. B. Brogan, K. H. Jensen, and R. J. Nelson, “Sub-synchronous control interaction studies between full-converter wind turbines and series-compensated ac transmission lines,” *IEEE Power Energy Soc. Gen. Meet.*, pp. 1–5, 2012, doi: 10.1109/PESGM.2012.6345523.

[15] J. S. Pascual and E. G. Villabona, “Diseño de un Convertidor Multimegavatio en Configuración Paralelo para Aplicación Eólica,” España, p. 108, 2015.

[16] Y. Xu, M. Zhang, L. Fan, and Z. Miao, “Small-Signal Stability Analysis of Type-4 Wind in Series Compensated Networks,” pp. 1–10.

[17] M. Davari and Y. A. R. I. Mohamed, “Robust DC-Link Voltage Control of a Full-Scale PMSG Wind Turbine for Effective Integration in DC Grids,” *IEEE Trans. Power Electron.*, vol. 32,

no. 5, pp. 4021–4035, 2017, doi: 10.1109/TPEL.2016.2586119.

[18] P. Paitandy and S. Mishra, “Nonlinear Disturbance Observer Based DC-Link Voltage Control for Grid-Connected VSC,” *3rd Int. Conf. Energy, Power Environ. Towar. Clean Energy Technol. ICEPE 2020*, pp. 0–4, 2021, doi: 10.1109/ICEPE50861.2021.9404400.

[19] B. Dhouib, A. Kahouli, and H. H. Abdallah, “Dynamic behavior of grid-connected fixed speed wind turbine based on proportional-integral pitch controller and fault analysis,” *Int. Conf. Green Energy Convers. Syst. GECS 2017*, 2017, doi: 10.1109/GECS.2017.8066242.

[20] V. Sandeep, V. Bala Murali Krishna, K. K. Namala, and D. N. Rao, “Grid connected wind power system driven by PMSG with MPPT technique using neural network compensator,” *2016 Int. Conf. Energy Effic. Technol. Sustain. ICEETS 2016*, pp. 917–921, 2016, doi: 10.1109/ICEETS.2016.7583879.

[21] S. Vajpayee, N. R. Panda, and P. Behera, “Crowbar protection of grid connected double fed induction generator with variable speed wind turbine,” *Proc. 2nd Int. Conf. Commun. Electron. Syst. ICCES 2017*, vol. 2018-Janua, no. Icces, pp. 56–61, 2018, doi: 10.1109/CESYS.2017.8321158.

[22] F. Asghar, “Variable Speed Externally Excited Synchronous Generator Drive for Wind Turbine Applications,” no. August 2016, p. 8, 2020.

[23] H. Li, “An Improved Grid-connected Control Strategy of Double PWM Direct-drive Permanent-magnet Synchronous Wind Generators,” *2nd Int. Conf. Smart Grid Smart Cities, ICSGSC 2018*, pp. 105–110, 2018, doi: 10.1109/ICSGSC.2018.8541277.

[24] S. Celikdemir and M. Ozdemir, “Wind Power Plant Application with Permanent Magnet Synchronous Generator,” *Proc. - 2019 4th Int. Conf. Power Electron. their Appl. ICPEA 2019*, no. September, pp. 25–27, 2019, doi: 10.1109/ICPEA1.2019.8911170.

[25] S. Li, T. A. Haskew, E. Muljadi, and C. Serrentino, “Characteristic study of vector-controlled direct-driven permanent magnet synchronous generator in wind power generation,” *Electr. Power Components Syst.*, vol. 37, no. 10, pp. 1162–1179, 2009, doi: 10.1080/15325000902954052.

[26] B. Wu, *Modeling and Modern Control of Wind Power*, 1er ed. Wiley-IEEE, 2018.

[27] L. Fan, *Control and Dynamics in Power Systems and Microgrids*, 1st, ed. vol. 1. Boca Raton, 2017.

[28] L. Fan, “Modeling Type-4 Wind in Weak Grids,” *IEEE Trans. Sustain. Energy*, vol. 10, no. 2, pp. 853–864, 2019, doi: 10.1109/TSTE.2018.2849849.

[29] L. Fan and Z. Miao, “Wind in Weak Grids: 4 Hz or 30 Hz Oscillations?,” *IEEE Trans. Power Syst.*, vol. 33, no. 5, pp. 5803–5804, 2018, doi: 10.1109/TPWRS.2018.2852947.